Chemical Geology 524 (2019) 228–236

Contents lists available at ScienceDirect

Chemical Geology

journal homepage: www.elsevier.com/locate/chemgeo

The significant effect of photo-catalyzed redox reactions on the immobilization of chromium by hematite

Jing Liu[a,b,c], Runliang Zhu[a,b,c,*], Qingze Chen[a,b,c], Huijun Zhou[a,b,c], Xiaoliang Liang[a,b,c], Lingya Ma[a,b,c], Steve C. Parker[d]

[a] CAS Key Laboratory of Mineralogy and Metallogeny/Guangdong Provincial Key Laboratory of Mineral Physics and Materials, Guangzhou Institute of Geochemistry, Chinese Academy of Sciences (CAS), Guangzhou 510640, China
[b] University of Chinese Academy of Sciences, Beijing 100049, China
[c] Institutions of Earth Science, Chinese Academy of Sciences, Beijing 100029, China
[d] Department of Chemistry, University of Bath, Claverton Down, Bath BA2 7AY, UK

ARTICLE INFO

Editor: Karen Johannesson

Keywords:
Hematite
Natural semiconductors
Chromium
Photo-catalyzed redox reactions
Adsorption

ABSTRACT

Naturally occurring semiconducting metal (oxyhydr)oxides (MeO_x) are ubiquitous geosorbents and geocatalysts, regulating the geochemical behaviors of the chemicals in the environment. The interactions between these MeO_x and redox-sensitive elements may involve both the photo-catalytic redox reactions and surface adsorption, and the interplay of the two processes, therefore, makes the interactions rather complex and may have unique environmental effects. The complex interactions between Cr (Cr(III) or Cr(VI)) and hematite under simulated sunlight irradiation were systematically studied under different geochemical conditions (pH, light irradiation, beginning Cr species, etc.). The batch experimentals, X-ray photoelectron spectroscopy (XPS), transmitted electron microscopy (TEM), and energy-dispersive spectroscopy (EDS) were used to determine the concentration and distribution of Cr species (Cr(III), Cr(VI), or the sum of the two) in the aqueous and solid phases. Here we found that both the oxidation of Cr(III) and the reduction of Cr(VI) were accelerated by hematite under sunlight irradiation, resulting in the enhanced immobilization of Cr on hematite. The reduction and oxidation efficiencies were pH-dependent and more evident under acidic condition. In the Cr (III) reaction systems, the reactions can be characterized by (1) the adsorption of aqueous Cr(III) ($Cr(III)_{aq}$) to hematite surfaces, (2) the oxidation of adsorbed Cr(III) ($Cr(III)_{ad}$) to $Cr(VI)_{ad}$ by the photogenerated holes on hematite, i.e., heterogeneous oxidation, (Bargar et al., 1997) the accumulation of $Cr(III)_{ad}$ on hematite enhanced by $Cr(VI)_{ad}$, and even the formation of Cr-riched precipitation, which was observed by TEM, and (3) the homogeneous oxidation of $Cr(III)_{aq}$ to $Cr(VI)_{aq}$ by the hydroxyl radicals, generating through interaction between O_2 and the photogenerated electrons (more evident under acidic environment, e.g., pH 3). In the Cr(VI) reaction systems, the reduction of $Cr(VI)_{ad}$ by photogenerated electrons from hematite was also noticeable, with the yielded Cr(III) being fixed on the surfaces. Although the reactions in reduction systems were less extensive than those in the oxidation systems, the reduction reactions would reduce the environmental toxicity of Cr species; while in the oxidation systems, inspite of the higher removal efficiency, the oxidation processes actually increased the environmental risk of Cr. Our results clearly show that hematite could either oxidize Cr(III) or reduce Cr(VI), influencing the speciation and immobilization of Cr under sunlight irradiation. In this term, the natural semiconducting MeO_x (e.g., hematite) on Earth's surfaces should play a significant role in affecting the environmental behaviors and toxicities of the redox-sensitive elements (e.g., Cr) through adsorption and photo-catalytic redox processes.

1. Introduction

Natural semiconducting metal (oxyhydr)oxides (MeO_x), such as titanium, manganese, and iron (oxyhydr)oxides (TiO_x, MnO_x, and FeO_x), are important components of the Earth's near-surface environment (Xu and Schoonen, 2000; Becker et al., 2001; Xu et al., 2013; Doane, 2017). Many of these MeO_x are in nano−/micro-scale size with large specific surface areas and abundant reactive functional groups; besides, they

* Corresponding author at: CAS Key Laboratory of Mineralogy and Metallogeny/Guangdong Provincial Key Laboratory of Mineral Physics and Materials, Guangzhou Institute of Geochemistry, Chinese Academy of Sciences (CAS), Guangzhou 510640, China.
E-mail address: zhurl@gig.ac.cn (R. Zhu).

https://doi.org/10.1016/j.chemgeo.2019.06.005
Received 30 January 2019; Received in revised form 28 May 2019; Accepted 5 June 2019
Available online 14 June 2019

can generate electron-hole pairs under sunlight irradiation (Xu and Schoonen, 2000; Zhu et al., 2018a, 2018b). As a result, these semiconducting minerals may play critical roles in a wide variety of geochemical processes, such as the adsorption of natural chemicals (Fosso-Kankeu et al., 2016; Di Iorio et al., 2018) and the exchange of electrons with various chemicals and microorganisms (Becker et al., 2001; Shi et al., 2016). Hence, they have been recognized as essential geosorbents and geocatalysts in the Earth's near-surface environment.

The adsorption of the natural chemicals on the MeO_x have been illustrated by plenty of studies and various adsorption mechanisms have been derived, including electrostatic attraction, hydrogen bonding, ligand exchange, surface precipitation, etc. For instance, Sr(II) was adsorbed on hematite surfaces as monodentate inner-sphere complexes (Olga et al., 1999); Pb(II) formed edge-sharing complexes on goethite and hematite (Bargar et al., 1997); Ca(II) and Mg(II) were adsorbed as outer-sphere complexes on iron and manganese oxides (Kinniburgh et al., 1983; Antelo et al., 2015). In many cases, multiple mechanisms can be simultaneously involved. For example, a transition of inner-sphere complexes to surface precipitation was found on goethite surface with the enhanced loading amounts of Cr(III) (Charlet and Manceau, 1992). Interestingly, as many of the MeO_x are nano − /micro-sized particles and have high mobility in nature, they could act as important shuttles in transporting the adsorbed chemicals in the nature, helping the long-distance transportation of various chemicals (Cornell and Schwertmann, 2003; Caraballo et al., 2014). One good example is the transport of FeO_x with surface-bound metals (e.g., Zn and Pb) to kilometers downstream from the mining sites in western Montana, USA (Hochella et al., 2005). In this term, the adsorption of chemicals on MeO_x is recognized as an important pathway affecting their migration.

On the other hand, some concurrent studies indicated that under sunlight irradiation the semiconducting MeO_x could catalyze many light-driven reactions in Earth's surface environment (Doane, 2017). The decomposition of organic contaminants and redox of inorganic contaminants in the environment can be accelerated by these semiconducting minerals under light irradiation (Li et al., 2006; Han et al., 2011; Doane, 2017). For example, the formation of hydroxyl radical and efficient photodegradation of organic compounds (e.g., 2-aminophenol) in illuminated suspensions of goethite were observed (Andreozzi et al., 2003; Han et al., 2011). Natural anatase was reported to accelerate the oxidation of chloride to perchlorate under light irradiation, supporting an alternative explanation for the high concentration of perchlorate on Mars (Schuttlefield et al., 2011). The light-induced redox of metal cations has raised considerable concerns as well, and the heterogeneous photo-catalytic reduction of Cr(VI) and oxidation of As(III) by TiO_2, ZnO, or Fe_2O_3 under light irradiation were frequently studied (Ferguson et al., 2005; Chakrabarti et al., 2009; Qiu et al., 2012; Wang et al., 2016b). Despite that the objective of many of these studies focused on environmental remediation of the redox-sensitive metals, similar reactions may be of high importance in controlling the speciation and geochemical transport of these metals in the nature as well.

Although the roles of MeO_x acting as geosorbents and geocatalysts have been extensively studied, most of previous studies only focused on one aspect (Yang et al., 2014; Doane, 2017; Di et al., 2018). Indeed, under many circumstances, surface adsorption and photo-catalytic redox of ions may concurrently occur on the surfaces of these minerals in the nature. The redox processes of elements usually include the change of the geometry (AsO_3^{3-} vs. AsO_4^{3-}) or the reverse of ionic charge (Cr^{3+} vs. CrO_4^{2-}) of the ions (Power et al., 2005; Tang et al., 2014; Yang et al., 2015; Tomaszewski et al., 2017), which may lead to attendant variations on the complexation of the elements on the surfaces of minerals. For instance, Morin et al. (2008) proposed that arsenate and arsenite showed varied adsorption behaviors on maghemite; Feng et al. (2018) found the coupled oxidation and adsorption/desorption of As(III) to MnO_2 was complex, and they provided a quantitative modeling framework for the initial stages of reaction. One could imagine that the uptake of redox-sensitive chemicals would become rather complex due to the redox of the chemicals under light irradiation: on one hand, the affinity between the mineral surfaces and the adsorbed species can be quite different as the valence of the ions changes; on the other hand, the adsorbed species could further modify the surface charge potentials and the surface reactive sites of minerals, affecting the subsequent interactions of the mineral surfaces and the aqueous species in the solution. Indeed, a number of related co-adsorption studies on minerals surfaces, in which the co-existence of multiple species (especially with opposite charges) can lead to either synergistic (Elzinga and Kretzschmar, 2013; Liu et al., 2016; Liu et al., 2018) or antagonistic adsorption (Benjamin and Leckie, 1982), revealed the significant effects of co-adsorbed ions on the surface properties of minerals. In this context, the interactions between redox-sensitive ions and the surfaces of semiconducting minerals under sunlight irradiation should be a comprehensive result of the variations in the electrovalence of ions and the surface properties of minerals. Hence, understanding how the combined processes of photo-catalytic redox and surface adsorption of ions induced by semiconducting minerals affect the geochemical behaviors of the redox-sensitive ions is of high necessity.

Among the various redox-sensitive ions in the environment, Cr has raised particular concerns due to its wide distribution and high toxicity. The two primary forms of Cr (i.e., Cr(III) and Cr(VI)) have quite different toxicity and mobility (Døssing et al., 2011; Zhitkovich, 2011; Wang et al., 2016a) and may interchange under natural conditions. Cr (VI) in nature can be reduced by microorganisms, chemical compounds and minerals with reducing capacity (Singh et al., 2017), or semiconductors with sunlight irradiation (e.g., TiO_2 and Fe_2O_3) (Mekatel et al., 2012; Qiu et al., 2012). By contrast, the oxidation of Cr(III) has been considered to be quite difficult. It is generally believed that Cr(III) could only be directly oxidized by those strong natural oxidants (e.g., manganese oxides, hydroxyl radicals, or hydrogen peroxide) (Pettine and Frank, 1990; Yang et al., 2014) or photo-oxidized when chelated with the organic acids (e.g., EDTA or citric acid) (Cieśla et al., 2004; Dai et al., 2010; Dai et al., 2011); recently, Tang et al. (2014) proposed that the oxidation of Cr(III) by MnO_x would continuously happen with the secondary MnO_x produced in the presence of organics and light irradiation. However, the effects of ubiquitously distributed semiconducting minerals on the redox, removal, and the consequent environmental toxicity of Cr under sunlight irradiation are still elusive.

In this study, Cr is used to probe the comprehensive effects of semiconducting MeO_x on the migration and transformation of the redox-sensitive pollutants in the surficial environment. Hematite is selected as representative semiconducting MeO_x as it is the most stable polymorph of FeO_x and distributed ubiquitously in the environment; besides, its good optical absorption bands in the UV and near IR region made it a unique solar energy harvester (Bora et al., 2013). The photocatalytic oxidation of Cr(III) and reduction of Cr(VI) by hematite under simulated sunlight irradiation, as well as the corresponding immobilization of the Cr species on the surfaces of hematite, were investigated under various environmentally related conditions.

2. Materials and experiments

2.1. Materials

$Cr(NO_3)_3$•$9H_2O$ was purchased from Shanghai Macklin Reagent Co., LTD; $K_2Cr_2O_7$, isopropanol, NaOH, and HNO_3 were bought from Guangzhou Chemical Reagent Factory; hematite was purchased from Shanghai Aladdin Bio-Chem Technology Co., LTD. All of the solutions were prepared using ultrapure water with a resistivity of 18 MΩ•cm. All of the glassware and quartz tubes were cleaned by soaking in 1 M HCl for overnight before used.

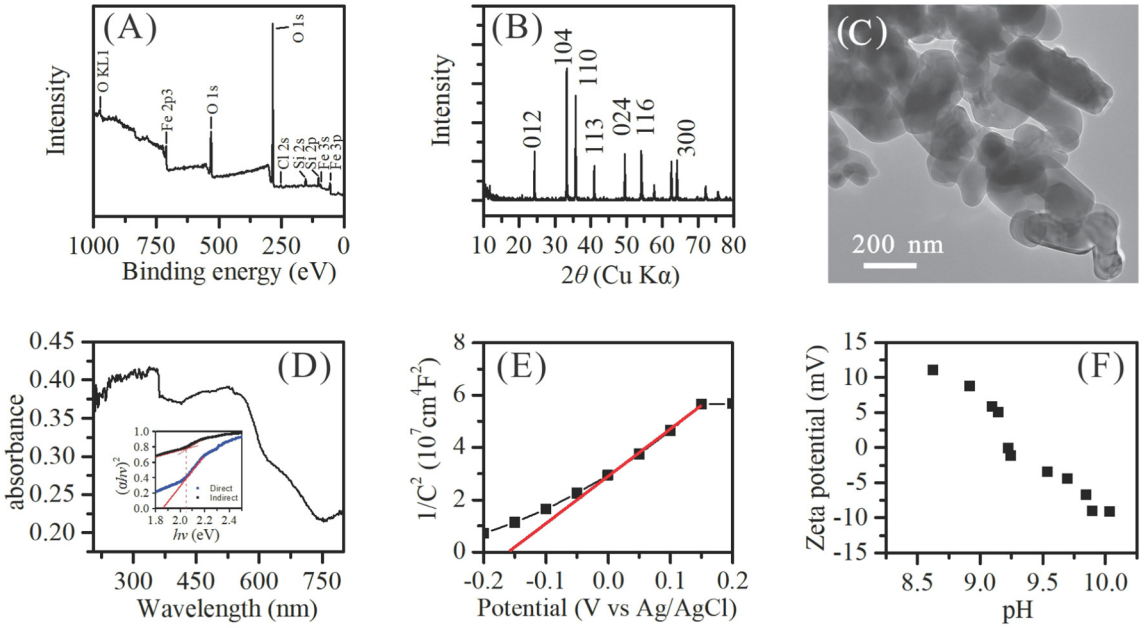

Fig. 1. Characterization of hematite. (A) XPS (X-ray photoelectron spectroscopy) survey spectrum of hematite (the peaks in the range of 710–1000 eV are auger peaks of Fe and O; the Cl should be residue in the synthesis process; the Si was derived from the tape that was used in the preparation of XPS sample). (B) XRD pattern of hematite. (C) Transmission electron microscopy (TEM) image of hematite showing irregular particles with varied diameters. (D) Mott-Schottky (MS) plot of hematite (the plot was measured using a three-electrode system at room temperature with hematite photo-anode as the working electrode and an Ag/AgCl electrode as the reference electrode). (E) The ultraviolet-visible diffuse reflectance spectrum of hematite (the inset shows the direct and indirect Tauc plots). (F) Zeta potential of hematite surfaces under different solution pH.

2.2. Characterization

X-ray diffraction (XRD) pattern of the hematite was acquired by Bruker D8 ADVANCE X-ray diffractometer (Karlsruhe, Germany). The measurement was performed at 40 kV and 40 mA with Cu Kα irradiation. X-ray photoelectron spectroscopy (XPS) analyses were carried out using a Thermo Fisher Scientific K-Alpha spectrometer (Waltham, USA). To compensate for the charging effects, all of the spectra were calibrated using the C 1 s peak with a fixed binding energy of 284.8 eV. Zeta potential measurements of hematite were carried out with a Malvern Zetasizer Nano-ZS (UK). Specifically, 0.05 g of the samples was added to 20 mL of 1 mM $NaNO_3$ solution. The pH of the suspension was adjusted using 1 M HNO_3 and NaOH solutions. The pH was measured by a pH-meter (PHS-3C, Shanghai LeiCi, China).

The photo-electrochemical measurements were performed with a CHI 660E electrochemical workstation (CH Instruments, Inc. USA). The Mott-Schottky plot was obtained using a three-electrode system at room temperature. The electrolyte was a 0.5 M Na_2SO_4 solution at pH 5, and the 1000 W Xe lamp was used as the light source. The optical properties of the hematite were measured by a UV–visible diffuse reflectance spectrophotometer (DRS) (UV-2550, Shimazu, Japan), in which $BaSO_4$ was employed as the internal reflectance standard.

Transmitted electron micrograph (TEM) and the high-resolution TEM (HRTEM) was collected on FEI Talos F200S (USA), operated at an accelerating voltage of 200 kV. The suspensions were collected at the reaction endpoint in each system and washed using dialysis treatment. The specimens were prepared by placing a drop of the dispersed suspension after ultrasonic treatment for 0.5 min on a porous carbon film supported by a copper grid, and the TEM grids were observed after the evaporation of water.

2.3. Photo-catalytic redox reactions

The light-induced redox reaction experiments were conducted in a photochemical reaction instrument (BL-GHX-V, Shanghai Depai Biotech. Co. Ltd., China). A 1000 W xenon lamp (100–105 mW/cm^2) was used as the simulated sunlight source, which was placed in a cylindrical Pyrex vessel surrounded by a circulating water jacket. Appropriate amounts of the Cr(III) or Cr(VI) stock solutions were added to the quartz tubes, and the volumes of the mixed solutions were set to 50 mL. Afterward, 0.05 g of hematite powder was added to the solution. The concentrations of Cr(III) or Cr(VI) in the solution before reactions were 0.2 mM (the initial concentrations of Cr in each reaction systems were tested and presented in Table S1). The pH of the solutions was adjusted to 3–5 using NaOH or HNO_3 (1 M). As 0.2 mM of Cr(III) solution could form precipitation under pH 4.8, the pH values of the Cr (III) were adjusted to pH 3, pH 3.8, and pH 4.6. The control experiments under dark condition were conducted using the same setting without irradiation. Precipitation of Cr(III) under the experimental conditions can be eliminated based on the thermodynamic calculations using Visual Minteq 3.0. To determine the effects of O_2 and hydroxyl radicals on the oxidation of Cr, reactions under anaerobic condition and in the presence of hydroxyl radical scavenger were investigated, respectively. In the anaerobic experiment, O_2 in the aqueous solutions was first eliminated by bubbling O_2-free N_2 gas overnight; afterward, the suspensions for reaction was prepared according to the procedures conducted in the aerobic experiment. During the reactions, O_2 in the air was isolated by continuously bubbling O_2-free N_2 gas through the suspensions. In the hydroxyl scavenging experiment, 50 mM of isopropanol was included in the suspensions as scavenger of hydroxyl radical (•OH) with the other conditions being the same to the experiment in the absence of hydroxyl radical scavenger.

In the kinetic reaction experiments, 1 mL of sample was taken out and filtered through 0.22 μm filter membranes to acquire the supernatant for further analysis. The concentrations of Cr(VI) were measured according to the diphenyl carbazide (DPC) method using an UV–vis spectrophotometry at 540 nm (759S, Shanghai JingHua Instrument Co. Ltd., China), and the concentrations of the total Cr (Cr(III) and Cr(VI)), were determined by atomic absorption spectroscopy (AAS) (Perkin Elmer AAnalyst 400, USA). The concentration of a Cr(VI) solution measured by UV–vis was within 5% of the concentration of Cr determined by AAS, indicating that the Cr concentrations measured using

the two methods are consistent and comparable. To compensate the differences in concentration measured by the two methods, the concentrations in each time point were divided by the initial concentration measured by the corresponding methods.

3. Results and discussion

3.1. Characterization of hematite

The XPS survey spectrum (Fig. 1A) reveals that the hematite primarily contained Fe and O, with a trace amount of chlorine. The XRD pattern of hematite (Fig. 1B) confirms the pure phase of α-Fe_2O_3 (JCPDS, No. 89–0598). The TEM (Fig. 1C) and SEM (Fig. S1) images show that the used hematite was composed of irregular particles with diameters ranging from dozens to hundreds of nanometers. The hematite could absorb light in the range between 200 and 800 nm, as shown in the DRS spectrum (Fig. 1D), and the calculated indirect and direct band gaps using Tauc eq. (S1) were ~2.05 and 1.85 eV, respectively. The Mott-Schottky plot (Fig. 1E) suggests that at pH 5, the measured potential vs. Ag/AgCl reference electrode was ~ − 0.156 V, which was ~ − 0.356 V in reversible hydrogen electrode (RHE) scale. The positive tangent of the slope indicates that hematite was an n-type semiconductor. Using the band gap value of 2.05 eV and conduction band potential of ~ − 0.356 V, the valence band value of hematite should be ~1.69 V, corresponding to those reported results (Lindgren et al., 2002; Bora et al., 2013). The point of zero charge of hematite was at ~pH 9.2 (Fig. 1F), indicating that the surfaces should be positively charged under most environmental conditions.

3.2. The reactions of Cr(III) with hematite under sunlight irradiation

3.2.1. The removal amounts and oxidation efficiencies of Cr(III) upon reaction with hematite

The removal of aqueous Cr(III) ($Cr(III)_{aq}$) in Cr(III) reaction systems (i.e., starting with only $Cr(III)_{aq}$ in the systems) by hematite was firstly investigated under dark condition (Fig. S2A). $Cr(III)_{aq}$ could be adsorbed by hematite and the removal percentages of $Cr(III)_{aq}$ increased from < 5% to ~10% as pH increasing from 3 to 4.6. The enhanced adsorption of $Cr(III)_{aq}$ with rising pH should be attributed to the decrease of the surface charge potential of hematite (i.e., less positive charge on the surface), as well as the formation of the hydrolysis products of $Cr(III)_{aq}$ at higher pH condition (Fig. S3), which could significantly enhance the ions reactivity by disrupting the symmetric water coordination sphere (Schindler and Stumm, 1987). On the other hand, as the adsorption equilibrium could be reached within 60 min (Fig. S2A), the suspensions were mixed under dark condition for 60 min before they were exposed to light irradiation in the following simulated sunlight experiments.

Under simulated sunlight irradiation, the removal of aqueous Cr (Cr_{aq}) (including both $Cr(III)_{aq}$ and $Cr(VI)_{aq}$) in the Cr(III) reaction systems evidently increased (Fig. 2A), with the removal efficiencies of ~11%, 25%, and 42% after irradiation for 120 min at pH 3, pH 3.8, and pH 4.6, respectively. At pH 3, the concentration of Cr_{aq} reached equilibrium after irradiation for 90 min, whereas it declined continuously under sunlight irradiation at pH 3.8 and pH 4.6. The reasons for this difference will be discussed below. The concentrations of $Cr(VI)_{aq}$ in the corresponding reaction systems (Fig. 2B) were examined to determine the amounts of different Cr_{aq} species (i.e., $Cr(III)_{aq}$ and $Cr(VI)_{aq}$). No detectable $Cr(VI)_{aq}$ was found in all of the systems under dark condition. On the other hand, the concentration of $Cr(VI)_{aq}$ strongly depended on solution pH under light irradiation: it remained almost undetectable in the system at pH 4.6 and then became quite noticeable as the solution pH decreased to 3.8. At pH 3, a sharp increase of $Cr(VI)_{aq}$ was observed after the suspension being irradiated for 20 min, and the concentration reached a platform at ~3.2 mg/L after 90 min. The presence of $Cr(VI)_{aq}$ confirmed the oxidation of Cr(III) under the

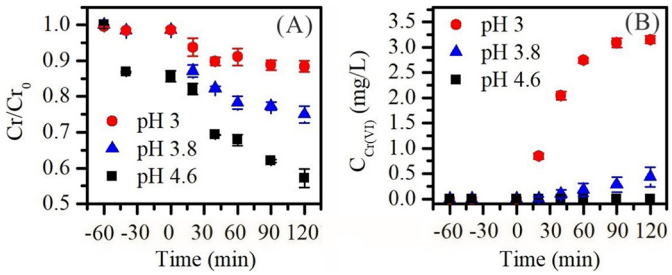

Fig. 2. Oxidation and immobilization of Cr(III) by hematite at different solution pH. (A) The removal kinetics of total Cr in the Cr(III) reaction systems in the presence of hematite under simulated sunlight irradiation (the initial concentration of Cr(III), as well as the concentration of the total Cr, were 0.2 mM (i.e., 11 mg/L)). (B) The concentration of aqueous Cr(VI) in the corresponding systems with different solution pH (the concentration of Cr(VI) was determined using ultraviolet-visible spectrophotometer). All of the suspensions were firstly reacted for 60 min without irradiation until the adsorption reached equilibrium.

irradiation at pH 3 and 3.8.

The contents of Cr species on the solid phases (Cr_{ad}) after reaction in the Cr(III) systems under sunlight irradiation were roughly determined using XPS. The binding energies of Cr 2p3/2 for all of the samples after reaction in Cr(III) systems were centered at ~577 eV with a shoulder peak at ~579 eV (Fig. 3A), which corresponds to Cr(III) and Cr(VI) species (Zhang et al., 2017), respectively. Hence, a dominant amount of Cr(III) and a small amount of Cr(VI) were mobilized on the surfaces of hematite after reactions under sunlight irradiation. The peaks were deconvoluted into two components using Thermo Avantage, and the areas of these peaks were calculated to indicate the contents of different Cr_{ad} species. The ratios of $Cr(VI)_{ad}/Cr(III)_{ad}$ on the surfaces of hematite were estimated and shown in the XPS image. The ratios of $Cr(VI)_{ad}/Cr(III)_{ad}$ on hematite surfaces at pH 4.6 (0.14) were lower than those on pH 3.8 (0.32) and pH 3 (0.31). According to the results from XPS analysis and the direct determination of the contents of Cr_{aq} species, the oxidation efficiencies as well as the distributions of Cr species in the liquid and on solid phases were estimated (Table S2) and plotted (Fig. 3B). The obtained results show that Cr(III) could be oxidized by hematite at pH from 3 to 4.6 under sunlight irradiation, and rising pH led to the decrease of the oxidation efficiencies of Cr(III), which were ~31%, 11%, and 5.2% at pH 3, pH 3.8, and pH 4.6, respectively.

3.2.2. The photo-catalytic oxidation mechanisms of Cr(III) by hematite

Under simulated sunlight irradiation, the electrons can be excited from the valence band to the conduction band of hematite (Table 1, Eq. 1, 2, 3), generating photo-induced electrons and holes (Xu and Schoonen, 2000). At pH 3 and pH 4.6, the valence band potentials of hematite are ~1.81 and 1.69 V, and the redox potentials of Cr(VI)/Cr(III) are about 0.916 and 0.640 V, respectively (Qiu et al., 2012). Hence, the holes in the valence band are capable of oxidizing the adsorbed Cr(III) (Eq. 7). Generally, the light-induced electrons and holes in hematite will readily recombine (Eq. 4, 5, 6). Nevertheless, previous studies (Xu et al., 2016) proved that O_2 was an efficient scavenger of electrons, which could inhibit the recombination of electrons and holes in hematite; besides, when O_2 accepts electrons in the conduction band of hematite, some reactive oxygen species, such as HO_2•, H_2O_2, and •OH, could be generated (Eq. 8, 9, 10 and 11) (Li et al., 2016), which could also contribute to the oxidation of Cr(III). Hence, O_2 and the generated reactive oxygen species might play important roles in the oxidation of Cr(III).

To understand the effects of O_2 on the photo-catalytic oxidation of Cr(III), experiments under anaerobic condition were conducted. The results (Fig. S4A) show that under anaerobic condition, the concentration of Cr was not evidently changed after light irradiation and Cr (VI) was not detected in solution. The XPS analysis (Fig. 3A) indicates that the sample after reaction in anaerobic condition contained low

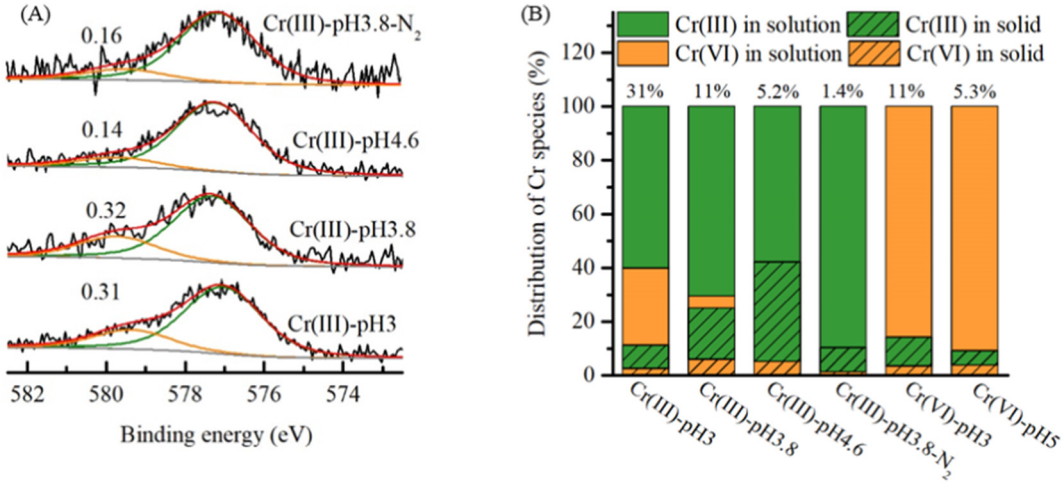

Fig. 3. (A) XPS spectra of Cr 2p3/2 in the samples after reactions in the Cr(III) systems under sunlight irradiation. The numbers in the patterns denote the ratios of Cr (VI)/Cr(III) on hematite calculated according to the area of the resolved peaks. (B) Distribution histogram of Cr(III) and Cr(VI) in the liquid and on solid phases in the Cr(III) and Cr(VI) reaction systems. The numbers on the column are the oxidation/reduction efficiencies calculated according to the XPS analysis and the direct determination of the contents of aqueous Cr species.

Table 1
The major reactions involved in the redox of Cr(III) and Cr(VI) on hematite at pH 5 and the corresponding redox potentials.

Equation	Potentials (V)	No.
Charge separation		
$Fe_2O_3 + hv \rightarrow e_{CB}^- + h_{VB}^+$	–	1
Surface trapping		
$\equiv Fe^{III}OH + h_{VB}^+ \rightarrow \{\equiv Fe^{III}OH\cdot\}^+$	–	2
$\equiv Fe^{III}OH + e_{CB}^- \rightarrow Fe^{II}OH$	–	3
Recombination		
$e_{CB}^- + h_{VB}^+ \rightarrow$ heat	–	4
$e_{CB}^- + \{\equiv Fe^{III}OH\cdot\}^+ \rightarrow \equiv Fe^{III}OH$	–	5
$h_{VB}^+ + Fe^{II}OH \rightarrow \equiv Fe^{III}OH$	–	6
Interfacial charge transfer		
Oxidation		
$2Cr^{3+} + 6h^+ + 7H_2O \rightarrow 14H^+ + Cr_2O_7^{2-}$	–	7
$O_2 + H^+ + e^- \rightarrow HO_2\cdot$	−0.341	8
$O_2 + 2H^+ + 2e^- \rightarrow H_2O_2$	0.4	9
$O_2 + 4H^+ + 4e^- \rightarrow 2H_2O$	0.935	10
$H_2O_2 + e^- \rightarrow \cdot OH + OH^-$	≤0.6	11
Reduction		
$Cr_2O_7^{2-} + 6e^- + 8H^+ \rightarrow 2Cr^{3+} + 4H_2O$	0.64	12
$2H_2O + 4h^+ \rightarrow O_2 + 4H^+$	−0.935	13

concentration of Cr with the ratio of Cr(VI)/Cr(III) on the surfaces being 0.16 and the oxidation percentage being ~1.4% (Fig. 3B). The weak oxidation of Cr(III) under anaerobic condition could be attributed to the available photo-generated holes in hematite, which were rather limited. Hence, the oxidation of Cr(III) should be greatly inhibited in this anaerobic system, and O_2 and oxygen radicals should be vital factors in the oxidation of Cr(III). To find out the role of radicals in the oxidation processes, reaction in the presence of isopropanol (a •OH radical scavenger) was further investigated. The production of $Cr(VI)_{aq}$ was completely inhibited by 50 mM of isopropanol at pH 3.8 (Fig. S4A), and the same result was got at pH 3 as well (data not shown). The XPS spectrum (Fig. S4B) suggests that isopropanol had negligible effects on the oxidation of Cr(III) on hematite surfaces. In this term, isopropanol should solely inhibit the oxidation of Cr(III) in the solution, suggesting that the •OH primarily influenced the homogeneous oxidation of Cr(III). The higher concentration of $Cr(VI)_{aq}$ in oxidation systems under more acidic condition could be linked to the production of •OH, which would rise with the decreasing pH (Xu et al., 2013), and the oxidation ability of •OH, which could be stronger under acidic condition.

3.2.3. The environmental behaviors of Cr as affected by the oxidation reactions

It is worth noting that not only the amounts of Cr_{ad} on hematite surfaces were enhanced by simulated sunlight irradiation, but also the amounts of $Cr(III)_{ad}$ after sunlight irradiation were more than the equilibrium adsorbed amounts under dark condition. The $Cr(III)_{ad}$ amounts were ~3.0%–13% of the added Cr(III) before sunlight irradiation, whereas the $Cr(III)_{ad}$ after the reactions under sunlight irradiation were ~8.6%–37% of the added Cr(III) at pH 3–4.6. Hence, the $Cr(VI)_{ad}$ produced by the oxidation of $Cr(III)_{ad}$ should have further promoted the adsorption of $Cr(III)_{aq}$. At pH 3, the oxidation of Cr(III) was mainly through homogeneous reaction with a lot of $Cr(VI)_{aq}$ yielded; whereas at pH 3.8 and pH 4.6, more $Cr(III)_{aq}$ was adsorbed and in-situ oxidized to $Cr(VI)_{ad}$ on the surfaces of hematite, which could further increase the removal of $Cr(III)_{aq}$. This result also explains why the concentrations of Cr reached equilibrium in the removal kinetics at pH 3 while they decreased continuously at pH 3.8 and pH 4.6.

The distributions of the immobilized Cr on hematite were further detected using TEM. The hematite samples after the oxidation reactions did not undergo identifiable change both in the morphology and the crystal phase after the oxidation reactions, as shown by the TEM and HRTEM images (Fig. 4A and Fig. S5). The EDS elemental mapping images (Fig. 4B) display that hematite indeed served as a sink of Cr, as Cr was concentrated on hematite particles. It is interesting to note that the amorphous specimen in the marked area in Fig. 4A (as well as in Fig. S6) should be surface precipitates of Cr(III) on hematite at solution pH of 4.6, since it mainly contains Cr and O (Fig. S7). As both the solution pH (Table S3) and the concentration of $Cr(III)_{aq}$ decreased after the oxidation reactions, the bulk solution was still undersaturated with respect to the homogeneous precipitation; besides, such Cr-riched precipitates were not found in the sample after reaction in the same suspension under dark condition (Fig. S8). Hence, the precipitates should form due to the accumulation of Cr(III) on hematite surfaces induced by the simulated sunlight irradiation. Previous EXAFS studies (Charlet and Manceau, 1992) proposed that the Cr atoms in Cr(III) complexes adsorbed on goethite surfaces are surrounded by three metal (Fe or Cr) shells in a mixed α- and γ-MeOOH local structure (Me = Fe or Cr). Such polymers might act as nuclei for the precipitation of a surface hydrous Cr oxide when more $Cr(III)_{aq}$ were adsorbed to the surfaces. In spite that most of Cr were evenly distributed on the surfaces of hematite and only fragmentary precipitates were found on hematite, the formation of precipitates could effectively decrease the release of Cr from the surface and reduce the mobility of Cr. Therefore, the influence of

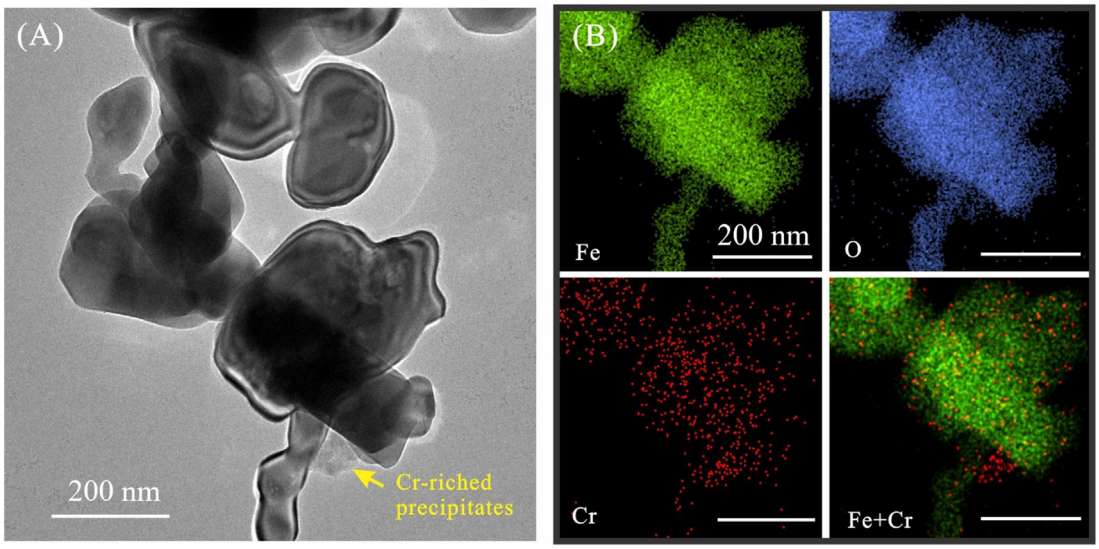

Fig. 4. (A) TEM images of the sample after reaction in Cr(III) system at pH 4.6 under sunlight irradiation and (B) the corresponding elemental mapping images showing the Cr-riched precipitates in the marked area. All scale bars are 200 nm.

hematite on the mobility and biotoxicity of Cr(III) under sunlight irradiation can be varied in different geological settings. Under most environmental pH conditions, the immobilization of Cr(III) can be enhanced and bioavailability of Cr species may be reduced due to the formation of precipitates on hematite under sunlight irradiation; however, under highly acidic environment, such as mine tailings, hematite may accelerate the transformation of $Cr(III)_{aq}$ to $Cr(VI)_{aq}$ by light-induced reaction, enhancing the environmental toxicity of Cr species.

3.3. The reactions of Cr(VI) with hematite under sunlight irradiation

3.3.1. The removal amounts and reduction efficiencies of Cr(VI) upon reaction with hematite

The removal amounts of $Cr(VI)_{aq}$ by hematite in the Cr(VI) reaction systems (i.e., starting with only $Cr(VI)_{aq}$ in the systems) under dark condition were extremely weak (below 5%) at pH 3 and pH 5, indicating the weak interaction between $Cr(VI)_{aq}$ and hematite under the experimental conditions. The weak affinity of Cr(VI) to hematite corresponds to the results of many previous studies about the adsorption of Cr(VI) on FeO_x (Chowdhury and Yanful, 2010; Troiano et al., 2013). Under simulated sunlight irradiation, the removal amounts of $Cr(VI)_{aq}$ and Cr_{aq} were accelerated (Fig. 5A), even though they were quite weak as compared with those of Cr_{aq} in the Cr(III) oxidation systems (Fig. 2A). After 120 min of sunlight irradiation, the removal

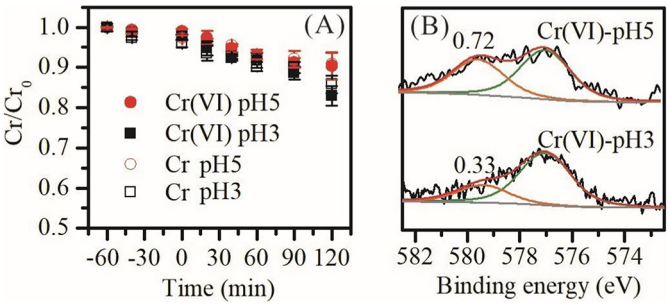

Fig. 5. Reduction and immobilization of Cr(VI) by hematite at different solution pH. (A) Removal kinetics of Cr(VI) and Cr in the Cr(VI) reaction systems at pH 3 and pH 5 in the presence of hematite under simulated sunlight irradiation. (B) XPS spectra of Cr 2p3/2 in the samples after reactions to the endpoint in Fig. A. The numbers in the XPS patterns denote the ratios of Cr(VI)/Cr(III) on hematite calculated according to the area of the resolved peaks.

percentages of $Cr(VI)_{aq}$ and Cr_{aq} at pH 5 were ~9.6% and 9.2%; whereas those at pH 3 were ~17% and 14%, respectively. The removal amounts of Cr_{aq} and $Cr(VI)_{aq}$ in the same systems were approximately equal, indicating that the solutions contain negligible quantities of $Cr(III)_{aq}$ after sunlight irradiation (i.e., completely immobilization of the reduced Cr).

The contents of Cr_{ad} species on the solid phases after reaction in the Cr(VI) systems under sunlight irradiation were determined using XPS (Fig. 5B), and the reduction of Cr(VI) on the surfaces of hematite was confirmed, as the peaks of Cr(III) were detected in the samples after the reaction. Besides, the amount of the $Cr(III)_{ad}$ was even higher than $Cr(VI)_{ad}$, as estimated according to the area of the peaks. At pH 3, the ratio of $Cr(VI)_{ad}/Cr(III)_{ad}$ was 0.33, and the corresponding reduction efficiency was about 11% (Fig. 3B). At pH 5, the ratio of $Cr(VI)_{ad}/Cr(III)_{ad}$ increased to 0.72, and the reduction efficiency descended to 5.3%. The results suggest that Cr(VI) could be reduced by hematite under sunlight irradiation, and the reduction was more efficient under acidic condition, similar to the oxidation of Cr(III). The immobilized amounts of $Cr(III)_{ad}$ and $Cr(VI)_{ad}$ on hematite after the reactions also indicate that hematite favored the uptake of $Cr(III)_{aq}$ even in the $Cr(VI)_{aq}$ enriched systems under acidic condition.

3.3.2. The photo-catalytic reduction mechanisms of Cr(VI) by hematite

Under simulated sunlight irradiation, $Cr(VI)_{ad}$ on hematite could be reduced to $Cr(III)_{ad}$ by the photo-generated electrons (Table 1, Eq. 12) after the hole-electron pairs being separated in hematite, and the holes may lead to production of O_2 (Eq. 13) (Li et al., 2016). The photo-catalytic reaction mainly included the three-electron-reduction of Cr(VI) to Cr(III) and the four-electron-oxidation of water to O_2, which are both kinetically slow; in addition, O_2 in the solution is able to compete for the photogenerated electrons and hence could inhibit the reduction of Cr(VI), since the redox potential of O_2 (0.935 V at pH 5) is higher than that of Cr(VI)/Cr(III) (Eq. 10). Once O_2 accept the electrons, the produced oxygen reactive radicals (e.g., hydroxyl radicals) could further oxidize the former generated Cr(III). Therefore, the photo-catalytic reduction of Cr(VI) on hematite was quite slow in this study. As suggested by the XPS analysis, the reduction efficiency of Cr(VI) was more evident under acidic condition, which could be attributed to the following two aspects: on one hand, the potentials of Cr(VI)/Cr(III) pair are ~0.916 V and 0.640 V at pH 3 and 5 (Wang et al., 2004), respectively; while the conduction band potentials are ~ − 0.238 V at pH 3 and − 0.356 V at pH 5, and hence the driving force for Cr(VI) reduction

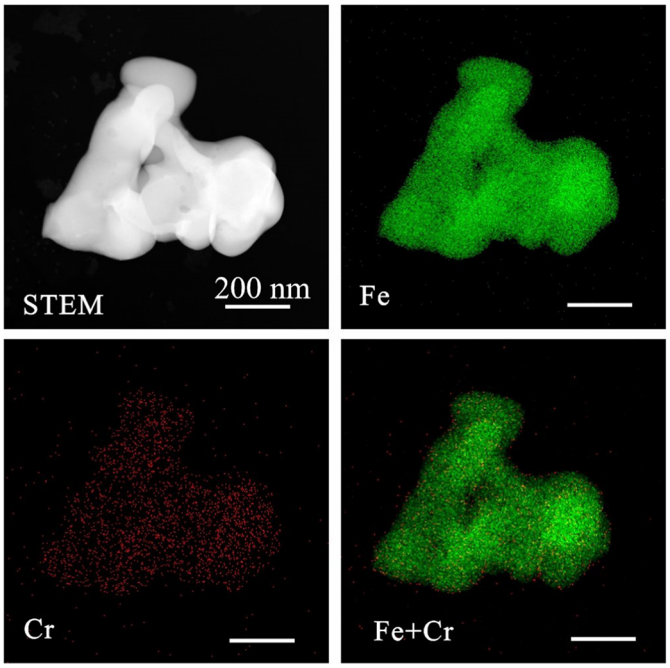

Fig. 6. Scanning transmission electron microscopy (STEM) image of the sample after reaction in Cr(VI) system at pH 5 and the corresponding elemental mapping images. All scale bars are 200 nm.

was higher at pH 3 than that at pH 5; on the other hand, as the reduction process would consume H^+ (Eq. 12), acidic condition with more H^+ would benefit the reduction of Cr(VI).

3.3.3. The environmental behaviors of Cr as affected by the reduction reactions comparison with the oxidation systems

The TEM and HRTEM images (Fig. S9) show that the hematite after the reduction reactions under sunlight irradiation at pH 5 were in similar morphology and the same crystal phase as compared to the samples before the reactions. As observed in the EDS elemental mapping images, Cr were concentrated and evenly distributed on hematite particles (Fig. 6); however, no evident precipitate was observed both in the EDS mapping and TEM images (Fig. S9), possibly due to the low concentration of Cr(III) on hematite. Although the removal amounts of the total Cr species were enhanced by sunlight irradiation, the amounts of $Cr(VI)_{ad}$ after reaction under sunlight irradiation were almost equal to the amounts of $Cr(VI)_{ad}$ before irradiation (Table S2), which were ~3.5%–3.9% of the added Cr(VI). Hence, the generated $Cr(III)_{ad}$ on hematite had negligible effect on the adsorption of the $Cr(VI)_{aq}$. The effects of the generated $Cr(III)_{ad}$ on the adsorption of $Cr(VI)_{aq}$ in the reduction systems are contrary to those in the oxidation systems, where the produced $Cr(VI)_{ad}$ evidently increased the immobilization of $Cr(III)_{aq}$ onto hematite. On the other hand, as shown in the supplementary experiment (Table S4), $Cr(III)_{aq}$ and $Cr(VI)_{aq}$ could not be synergistically adsorbed on hematite when they were co-existed. The differences could be related to the different affinity and bonding modes of Cr(III) and Cr(VI) to hematite surfaces, which will be discussed below.

Hematite favored the adsorption of $Cr(III)_{aq}$ over $Cr(VI)_{aq}$, as the removal ratios of Cr_{aq} species in the Cr(VI) systems were lower than those in the Cr(III) systems. This result agrees well with the conclusion drawn by Troiano et al. (2013): in spite that the surfaces of hematite were positively charged, their affinity to the cationic form (Cr^{3+} or $CrOH^{2+}$) was stronger than to the anionic form ($Cr_2O_7^{2-}$ or $HCrO_4^-$). The different affinities of hematite to the cations and anions forms of Cr might be related to the stability of the adsorbed complexes. Previous studies (Charlet and Manceau, 1992; Eggleston and Stumm, 1993) suggest that Cr(III) usually form strongly bound hydroxy polymers, and/or precipitates on FeO_x. These hydroxy polymers or precipitation could hardly affect the charge potential of hematite surfaces. Hence, the generated $Cr(III)_{ad}$ in the Cr(VI) reaction systems had negligible effects on the immobilization of $Cr(VI)_{aq}$. However, $Cr(VI)_{aq}$ had a weaker affinity to the FeO_x comparing to many oxyanions (e.g., phosphate and arsenate) (Pradhan et al., 1999; Chowdhury and Yanful, 2010) and often form outer-sphere complexes and a small quantity of inner-sphere complexes on ferrihydrite (Johnston and Chrysochoou, 2012), which might decrease the charge potential of mineral surfaces. Hence, in this study, the generated $Cr(VI)_{ad}$ benefited the adsorption of $Cr(III)_{aq}$ in the Cr(III) reaction systems; whereas in the Cr(VI) reaction systems, the yielded $Cr(III)_{ad}$ had negligible effects on the further adsorption of $Cr(VI)_{aq}$.

The photo-catalytic redox reactions in Cr(VI) solution were quite different from those in the Cr(III) solution, with respect to the reaction efficiencies and pathways. Although both the oxidation of Cr(III) and the reduction of Cr(VI) included interactions with the photo-generated holes (for oxidation) or electrons (for reduction) in hematite, the subsequent reactions coupling with the consumption of holes or electrons were varied. In Cr(III) solution, the interaction of $Cr(III)_{ad}$ with holes would lead to the accumulation of electrons in hematite, whose interaction with O_2 could yield highly oxidizing hydroxyl radicals or hydrogen peroxide, contributing to the homogeneous oxidation of $Cr(III)_{aq}$. However, the accumulation of holes as a result of the reduction of $Cr(VI)_{ad}$ by the photo-generated electrons with O_2 produced and the competition of O_2 (dissolved or produced) with Cr(VI) for electrons accompanying by the production of reactive oxygen species reduce the reduction efficiency. Comparing the results in the oxidation and reduction reaction systems, higher oxidation efficiencies of Cr(III) and removal amounts of total Cr species were found under sunlight irradiation in the Cr(III) enriched environment, and the consequent environmental toxicity of Cr was increased by the reactions of Cr(III) with hematite; whereas in the Cr(VI) enriched environment, although the reduction and removal of Cr species were less evident, such reactions could actually decrease the environmental risks of Cr species.

4. Conclusions

To the best of our knowledge, this is the first study exploring the speciation and migration of Cr as affected by hematite considering both the photo-catalytic redox and the adsorption processes under various geochemical conditions. Our results show that sunlight irradiation on the hematite suspensions could accelerate the oxidation of Cr(III) and reduction of Cr(VI), which were both accompanied by the enhanced immobilization of total Cr_{aq} at pH ranging ~3 to 5. In the Cr(III) enriched environment, $Cr(III)_{aq}$ could be fast adsorbed on hematite, and then on one hand the $Cr(III)_{ad}$ could be heterogeneously oxidized to $Cr(VI)_{ad}$ by the photo-generated holes on hematite; on the other hand, $Cr(III)_{aq}$ could be homogeneously oxidized to highly toxic $Cr(VI)_{aq}$ by the hydroxyl radicals yielded through interaction between O_2 and the electrons in the valence band of hematite. The produced $Cr(VI)_{ad}$ on hematite surfaces could stimulate further adsorption of $Cr(III)_{aq}$, which consequently led to the formation of Cr-riched surface precipitates as detected by TEM. In the Cr(VI) enriched environment, as a result of the weak interaction between $Cr(VI)_{aq}$ and the surfaces of hematite, small amounts of Cr(VI) were adsorbed and reduced to $Cr(III)_{ad}$ by accepting the photo-generated electrons in hematite. The reduction of Cr(VI) was weak as the available electrons were limited, and the production of O_2 in the oxidation of water by holes and reactive oxygen species by interaction of O_2 with electrons would hinder the reduction of Cr(VI). Nevertheless, the produced Cr(III) were entirely immobilized on hematite surfaces, and the removal of Cr increased by sunlight irradiation with the environmental toxicity being decreased. The results suggest that the migration and speciation of Cr in the natural environment could be influenced by hematite, especially under sunlight irradiation. Given the ubiquitous presence of FeO_x and that hematite is one of the

dominant FeO_x in the critical zone, the cycling scenario proposed in this study might play a significant role in controlling the speciation and immobilization of numerous redox-sensitive elements.

Acknowledgements

This is contribution No.IS-2721 from GIGCAS. This work was supported by the National Natural Science Foundation of China (41872044), the National Key Research and Development Plan of China (2016YFD0800704), and the Newton Advanced Fellowship (NA150190).

Appendix A. Supplementary data

Supplementary data to this article can be found online at https://doi.org/10.1016/j.chemgeo.2019.06.005.

References

Andreozzi, R., Caprio, V., Marotta, R., 2003. Iron(III) (hydr)oxide-mediated photooxidation of 2-aminophenol in aqueous solution: a kinetic study. Water Res. 37 (15), 3682–3688.
Antelo, J., Arce, F., Fiol, S., 2015. Arsenate and phosphate adsorption on ferrihydrite nanoparticles: Synergetic interaction with calcium ions. Chem. Geol. 410, 53–62.
Bargar, J.R., Brown, G.E., Parks, G.A., 1997. Surface complexation of Pb(II) at oxide-water interfaces: II. XAFS and bond-valence determination of mononuclear Pb(II) sorption products and surface functional groups on iron oxides. Geochim. Cosmochim. Acta 61 (13), 2639–2652.
Becker, U., Rosso, K., Hochella, M.F., 2001. The proximity effect on semiconducting mineral surfaces a new aspect of mineral surface reactivity and surface complexation theory. Geochim. Cosmochim. Acta 65 (16), 2641–2649.
Benjamin, M., Leckle, J., 1982. Effects of Complexation by Cl, SO_4, and S_2O_3 on Adsorption Behavior of Cd. Environ. Sci. Technol. 16, 162–170.
Bora, D.K., Braun, A., Constable, E.C., 2013. "In rust we trust". Hematite – the prospective inorganic backbone for artificial photosynthesis. Energy Environ. Sci. 6 (2), 407–425.
Caraballo, M.A., Michel, F.M., Hochella, M.F., 2014. The rapid expansion of environmental mineralogy in unconventional ways: beyond the accepted definition of a mineral, the latest technology, and using nature as our guide. Am. Mineral. 100 (1), 14–25.
Chakrabarti, S., Chaudhuri, B., Bhattacharjee, S., Ray, A.K., Dutta, B.K., 2009. Photoreduction of hexavalent chromium in aqueous solution in the presence of zinc oxide as semiconductor catalyst. Chem. Eng. J. 153 (1), 86–93.
Charlet, L., Manceau, A.A., 1992. X-ray absorption spectroscopic study of the sorption of Cr(III) at the oxide-water interface: II. Adsorption, coprecipitation, and surface precipitation on hydrous ferric oxide. J. Colloid Interface Sci. 148 (2), 443–458.
Chowdhury, S.R., Yanful, E.K., 2010. Arsenic and chromium removal by mixed magnetite–maghemite nanoparticles and the effect of phosphate on removal. J. Environ. Manag. 91 (11), 2238–2247.
Cieśla, P., Karocki, A., Stasicka, Z., 2004. Photoredox behaviour of the Cr-EDTA complex and its environmental aspects. J. Photochem. Photobiol. A Chem. 162 (2), 537–544.
Cornell, R.M., Schwertmann, C., 2003. The Iron Oxides: Structures, Properties, Reactions, Occurrences, and Uses. Wiley-VCH.
Dai, R., Yu, C., Liu, J., Lan, Y., Deng, B., 2010. Photo-oxidation of Cr(III) – Citrate complexes forms harmful Cr(VI). Environ. Sci. Technol. 44 (18), 6959–6964.
Dai, R., Yu, C., Gou, J., Lan, Y., Mao, J., 2011. Photoredox pathways of Cr(III)-tartrate complexes and their impacting factors. J. Hazard. Mater. 186 (2), 2110–2116.
Di Iorio, E., Cho, H.G., Liu, Y., Cheng, Z., Angelico, R., Colombo, C., 2018. Arsenate retention mechanisms on hematite with different morphologies evaluated using AFM, TEM measurements and vibrational spectroscopy. Geochim. Cosmochim. Acta 237, 155–170.
Doane, T.A., 2017. A survey of photogeochemistry. Geochem. Trans. 18 (1), 1.
Døssing, L.N., Dideriksen, K., Stipp, S.L.S., Frei, R., 2011. Reduction of hexavalent chromium by ferrous iron: a process of chromium isotope fractionation and its relevance to natural environments. Chem. Geol. 285 (1), 157–166.
Eggleston, C.M., Stumm, W., 1993. Scanning tunneling microscopy of Cr(III) chemisorbed on α-Fe_2O_3 (001) surfaces from aqueous solution: Direct observation of surface mobility and clustering. Geochim. Cosmochim. Acta 57 (19), 4843–4850.
Elzinga, E.J., Kretzschmar, R., 2013. In situ ATR-FTIR spectroscopic analysis of the coadsorption of orthophosphate and Cd(II) onto hematite. Geochim. Cosmochim. Acta 117, 53–64.
Feng, X., Wang, P., Shi, Z., Kwon, K.D., Zhao, H., Yin, H., Lin, Z., Zhu, M., Liang, X., Liu, F., Sparks, D.L., 2018. A quantitative model for the coupled kinetics of arsenic adsorption/desorption and oxidation on manganese oxides. Environ. Sci. Technol. Lett. 5 (3), 175–180.
Ferguson, M.A., Hoffmann, M.R., Hering, J.G., 2005. TiO_2-Photocatalyzed as(III) Oxidation in Aqueous Suspensions: Reaction Kinetics and Effects of Adsorption. Environ. Sci. Technol. 39 (6), 1880–1886.
Fosso-Kankeu, E., Waanders, F.B., Steyn, F.W., 2016. Removal of Cr(VI) and Zn(II) from an aqueous solution using an organic-inorganic composite of bentonite-biochar-hematite. Desalin. Water Treat. 59, 144–153.
Han, S.K., Hwang, T.M., Yoon, Y., Kang, J.W., 2011. Evidence of singlet oxygen and hydroxyl radical formation in aqueous goethite suspension using spin-trapping electron paramagnetic resonance (EPR). Chemosphere 84 (8), 1095–1101.
Hochella, M.F., Moore, J.N., Putnis, C.V., Putnis, A., Kasama, T., Eberl, D.D., 2005. Direct observation of heavy metal-mineral association from the Clark Fork River Superfund complex: Implications for metal transport and bioavailability. Geochim. Cosmochim. Acta 69 (7), 1651–1663.
Johnston, C.P., Chrysochoou, M., 2012. Investigation of chromate coordination on ferrihydrite by in situ ATR-FTIR spectroscopy and theoretical frequency calculations. Environ. Sci. Technol. 46 (11), 5851–5858.
Kinniburgh, D.G., Barker, J.A., Whitfield, M., 1983. A comparison of some simple adsorption isotherms for describing divalent cation adsorption by ferrihydrite. J. Colloid Interface Sci. 95 (2), 370–384.
Li, F., Chen, J., Liu, C., Dong, J., Liu, T., 2006. Effect of iron oxides and carboxylic acids on photochemical degradation of bisphenol a. Biol. Fertil. Soils 42 (5), 409–417.
Li, X., Yu, J., Jaroniec, M., 2016. Hierarchical photocatalysts. Chem. Soc. Rev. 45 (9), 2603–2636.
Lindgren, T., Wang, H., Beermann, N., Vayssieres, L., Hagfeldt, A., Lindquist, S., 2002. Aqueous photoelectrochemistry of hematite nanorod array. Sol. Energy Mater. Sol. Cells 71 (2), 231–243.
Liu, J., Zhu, R., Xu, T., Xu, Y., Ge, F., Xi, Y., Zhu, J., He, H., 2016. Co-adsorption of phosphate and zinc(II) on the surface of ferrihydrite. Chemosphere 144, 1148–1155.
Liu, J., Zhu, R., Liang, X., Ma, L., Lin, X., Zhu, J., He, H., Parker, S.C., Molinari, M., 2018. Synergistic adsorption of Cd(II) with sulfate/phosphate on ferrihydrite: an in situ ATR-FTIR/2D-COS study. Chem. Geol. 477, 12–21.
Mekatel, H., Amokrane, S., Bellal, B., Trari, M., Nibou, D., 2012. Photocatalytic reduction of Cr(VI) on nanosized Fe_2O_3 supported on natural Algerian clay: Characteristics, kinetic and thermodynamic study. Chem. Eng. J. 200–202, 611–618.
Morin, G., Ona-Nguema, G., Wang, Y., Menguy, N., Juillot, F., Proux, O., Guyot, F., Calas, G., Brown, G.E., 2008. Extended X-ray absorption fine structure analysis of arsenite and arsenate adsorption on maghemite. Environ. Sci. Technol. 42 (7), 2361–2366.
Olga, N.K., Ludmila, I.I., Leonid, Z.L., Lars, L., 1999. Strontium sorption on hematite at elevated temperatures. J. Colloid Interface Sci. 220, 419–428.
Pettine, M., Frank, J.M., 1990. Chromium speciation in seawater: the probable role of hydrogen peroxide. Limnol. Oceanogr. 35 (3), 730–736.
Power, L.E., Arai, Y., Sparks, D.L., 2005. Zinc adsorption effects on arsenite oxidation kinetics at the birnessite-water interface. Environ. Sci. Technol. 39 (1), 181–187.
Pradhan, J., Das, S.N., Thakur, R.S., 1999. Adsorption of hexavalent chromium from aqueous solution by using activated red mud. J. Colloid Interface Sci. 217 (1), 137–141.
Qiu, R., Zhang, D., Diao, Z., Huang, X., He, C., Morel, J.L., Xiong, Y., 2012. Visible light induced photocatalytic reduction of Cr(VI) over polymer-sensitized TiO_2 and its synergism with phenol oxidation. Water Res. 46 (7), 2299–2306.
Schindler, P.W., Stumm, W., 1987. The Surface Chemistry of Oxides, Hydroxides, and Oxide Minerals. John Wiley and Sons, New York, pp. 83–110.
Schuttlefield, J.D., Sambur, J.B., Gelwicks, M., Eggleston, C.M., Parkinson, B.A., 2011. Photooxidation of chloride by oxide minerals: implications for perchlorate on Mars. J. Am. Chem. Soc. 133 (44), 17521–17523.
Shi, L., Dong, H., Reguera, G., Beyenal, H., Lu, A., Liu, J., Yu, H., Fredrickson, J.K., 2016. Extracellular electron transfer mechanisms between microorganisms and minerals. Nat. Rev. Microbiol. 14 (10), 651–662.
Singh, R., Dong, H., Zeng, Q., Zhang, L., Rengasamy, K., 2017. Hexavalent chromium removal by chitosan modified-bioreduced nontronite. Geochim. Cosmochim. Acta 210, 25–41.
Tang, Y., Webb, S.M., Estes, E.R., Hansel, C.M., 2014. Chromium(III) oxidation by biogenic manganese oxides with varying structural ripening. Environ. Sci.: Processes Impacts 16 (9), 2127–2136.
Tomaszewski, E.J., Lee, S., Rudolph, J., Xu, H., Ginder-Vogel, M., 2017. The reactivity of Fe(II) associated with goethite formed during short redox cycles toward Cr(VI) reduction under oxic conditions. Chem. Geol. 464, 101–109.
Troiano, J.M., Jordan, D.S., Hull, C.J., Geiger, F.M., 2013. Interaction of Cr(III) and Cr(VI) with hematite studied by second harmonic generation. J. Phys. Chem. C 117 (10), 5164–5171.
Wang, X., Pehkonen, S.O., Ray, A.K., 2004. Removal of aqueous Cr(VI) by a combination of photocatalytic reduction and coprecipitation. Ind. Eng. Chem. Res. 43, 1665–1672.
Wang, H., Xu, X., Ren, Z., Gao, B., 2016a. Removal of phosphate and chromium(VI) from liquids by an amine-crosslinked nano-Fe_3O_4 biosorbent derived from corn straw. RSC Adv. 6 (53), 47237–47248.
Wang, J., Ren, J., Yao, H., Zhang, L., Wang, J., Zang, S., Han, L., Li, Z., 2016b. Synergistic photocatalysis of Cr(VI) reduction and 4-Chlorophenol degradation over hydroxylated α-Fe_2O_3 under visible light irradiation. J. Hazard. Mater. 311, 11–19.
Xu, Y., Schoonen, M.A.A., 2000. The absolute energy positions of conduction and valence bands of selected semiconducting minerals. Am. Mineral. 85, 543–556.
Xu, J., Sahai, N., Eggleston, C.M., Schoonen, M.A.A., 2013. Reactive oxygen species at the oxide/water interface: Formation mechanisms and implications for prebiotic chemistry and the origin of life. Earth Planet. Sci. Lett. 363, 156–167.
Xu, T., Zhu, R., Zhu, J., Liang, X., Liu, Y., Xu, Y., He, H., 2016. Ag_3PO_4 immobilized on hydroxy-metal pillared montmorillonite for the visible light driven degradation of acid red 18. Cat. Sci. Technol. 6 (12), 4116–4123.
Yang, F., Guo, J., Dai, R., Lan, Y., 2014. Oxidation of Cr(III)-citrate/tartrate complexes by δ-MnO2: production of Cr(VI) and its impact factors. Geoderma 213, 10–14.
Yang, N., Welch, K.A., Mohajerin, T.J., Telfeyan, K., Chevis, D.A., Grimm, D.A., Lyons, W.B., White, C.D., Johannesson, K.H., 2015. Comparison of arsenic and molybdenum geochemistry in meromictic lakes of the McMurdo Dry Valleys, Antarctica: Implications for oxyanion-forming trace element behavior in permanently stratified lakes. Chem. Geol. 404, 110–125.

Zhang, J., Zhang, C., Wei, G., Li, Y., Liang, X., Chu, W., He, H., Huang, D., Zhu, J., Zhu, R., 2017. Reduction removal of hexavalent chromium by zinc-substituted magnetite coupled with aqueous Fe(II) at neutral pH value. J. Colloid Interface Sci. 500, 20–29.
Zhitkovich, A., 2011. Chromium in drinking water: sources, metabolism, and cancer risks. Chem. Res. Toxicol. 24 (10), 1617–1629.
Zhu, Y., Zhu, R., Yan, L., Fu, H., Xi, Y., Zhou, H., Zhu, G., Zhu, J., He, H., 2018a. Visible-light Ag/AgBr/ferrihydrite catalyst with enhanced heterogeneous photo-Fenton reactivity via electron transfer from Ag/AgBr to ferrihydrite. Appl. Catal. B Environ. 239, 280–289.
Zhu, Y., Zhu, R., Xi, Y., Xu, T., Yan, L., Zhu, J., Zhu, G., He, H., 2018b. Heterogeneous photo-Fenton degradation of bisphenol a over Ag/AgCl/ferrihydrite catalysts under visible light. Chem. Eng. J. 346, 567–577.